

IR IMAGES TRANSFER THROUGH THE ATMOSPHERE

V.V. Belov, S.V. Afonin, and I.Yu. Makushkina

*Institute of Atmospheric Optics,
Siberian Branch of the Russian Academy of Sciences, Tomsk*

Received January 16, 1997

We discuss some results of investigations of outgoing thermal radiation of the "atmosphere – underlying surface system" in the 3–5 and 10–13 μm wavelength ranges, carried out based on the theory of linear systems. We also made more detailed analysis of the contribution coming from the process of scattering into the formation of upwelling thermal fluxes and its effect on the pulse response of the atmospheric optical channels of formation and transfer of IR images in addition to the results published earlier.

Special attention is paid to the slant paths of observation of the Earth's surface under the conditions of aerosol turbidity of tropospheric and stratospheric layers of the cloudless atmosphere. The result of numerical experiments simulating satellite observations of two types of the temperature-inhomogeneous underlying surface are presented as an example.

1. INTRODUCTION

The effect of the atmosphere on the Earth's surface images is the main factor that essentially limits or even excludes the possibility effective use of the aerospace data in different applications, including, for example, the geoinformation systems. This effect can be revealed in the image in different forms, from the change of the spectral pattern of the observed area of the surface, the distortion of the contrast and spatial structure and the object size to a complete or partial replacement of the ground object image with the atmospheric one (in the case of cloudiness, fog or aerosol).^{1,2} The processing of such aerospace data may contain significant errors in estimations of the parameters of the objects observed (temperature, color parameter or vegetation index, size of a fire or an oil spills, etc.).

One of the tendencies in the development and use of the optoelectronic complexes of aerospace observation of the Earth's surface in the geoinformation system network is related to the increase of their spatial, spectral and contrast sensitivity.³ On the one hand, it allows one to estimate the quantitative parameters of the observed processes or objects from these images more accurately and, on the other hand, that requires a more detailed and full knowledge of both the optical properties of the atmosphere and the mechanisms of formation of the images of the radiobrightness field observed through the multicomponent, nonstationary and, in general case, stochastic scattering and absorbing media.

For example, the atmospheric effect on the aerospace images of the low spatial resolution can be taken into account quite accurately using its integral

optical parameters (such as optical thickness, transmittance coefficient, etc.), but these data are insufficient for processing images of higher spatial resolution, and the additional information is needed about the fine spatial structure of the optical properties of the atmosphere. Moreover, the greater accuracy (spatial, temporal, spectral, etc.) is needed for reconstructing the parameters of the objects observed through the atmosphere, the more detailed information on its optical state should be taken into account when interpreting such images. In particular, this fact has attracted attention of the participants of the Conference on the Problems in Development and Application of Geoinformation Technologies (Siberian Branch of the Russian Academy of Sciences, Novosibirsk, March 19, 1996) and of the Third Inter-Republic Symposium "Atmospheric and Oceanic Optics" (Tomsk, July 2–5, 1996). These problems were also discussed at the International conference "Transfer of Images Through the Atmosphere" (SPIE, Denver, USA, August 7–9, 1996). The solution of these problems is the main goal of the program of the basic research at the Institute of Atmospheric Optics on the theory of formation and transfer of the images in light scattering media.

This paper generalizes the results of investigation of the formation of outgoing thermal radiation of the "atmosphere – underlying surface" system in the 3–5 and 10–13 μm wavelength ranges performed earlier by the authors and presented in details in Refs. 4–9.

The investigations were carried out based on the theory of linear systems. The more detailed analysis of the contribution of the scattering process into the formation of the upwelling thermal fluxes as well as

its effect on the pulse response of the atmospheric optical channels of formation and transfer of the IR images is proposed in addition to Refs. 4–9. The main attention is paid to the slant paths of observation of the Earth’s surface under the conditions of aerosol turbidity of tropospheric and stratospheric layers of the cloudless atmosphere. The relation is established between the characteristics of the secondary maximum of the pulse response and the optical and geometrical parameters of the slant paths of observation.

2. STATEMENT OF THE PROBLEM

Let the optical receiver aimed at the point M along the direction w_0 be situated at the point S (Fig. 1) which is at a distance H_0 from the spherical Earth’s surface of the radius R_E . There is a need to study the dependence of the optical radiation intensity J recorded with the receiver on the geometrical parameters of the observation optical arrangement (for example, on the angles φ and θ , the distance H_0 , etc.) and the optical properties of the multicomponent inhomogeneous cloudless atmosphere and the homogeneously reflecting (irradiating) Earth’s surface in the IR wavelength range ($\lambda = 3.75$ and $10.8 \mu\text{m}$). For solving this problem correctly it is necessary to take into account all physical processes contributing to the formation of the upwelling light fluxes in the direction of the receiver of radiation from the “atmosphere – underlying surface” system:

- scattering (including multiple scattering) and absorption of light by the aerosol and molecular constituents of the atmosphere;
- irradiation of the atmosphere;
- long-wave radiation of the Earth’s surface.

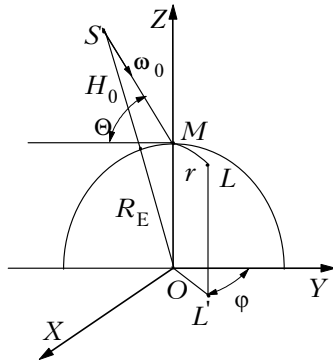


FIG. 1. Geometrical scheme used for modeling.

One can establish the relation between the intensity J and the optical and geometrical characteristics of the Earth’s surface and the atmosphere using the solution of the stationary equation of radiation transfer

$$(\mathbf{w}, \text{grad } J(\mathbf{r}, \mathbf{w})) = -\beta_{\text{ext}}(\lambda, \mathbf{r}) J(\mathbf{r}, \mathbf{w}) + \beta_{\text{sc}}(\lambda, \mathbf{r}) \int_{\Omega} J(\mathbf{r}, \mathbf{w}') g(\lambda, \mathbf{r}, \mathbf{w}, \mathbf{w}') d\mathbf{w}' + \Phi_0(\mathbf{r}, \mathbf{w}), \quad (1)$$

where $J(\mathbf{r}, \mathbf{w})$ is the intensity at the point r in the direction \mathbf{w} ; λ is the optical radiation wavelength; β_{ext} , $\beta_{\text{sc}}(\lambda, \mathbf{r})$, and $g(\lambda, \mathbf{r}, \mathbf{w}, \mathbf{w}')$ are the optical parameters of the medium; $\Phi_0(\mathbf{r}, \mathbf{w})$ is the inner radiation sources (for example, thermal radiation of the atmosphere). Let us write the boundary conditions for Eq. (1) in the form

$$\begin{cases} J(\mathbf{r}, \mathbf{w}) = S(\mathbf{r}, \mathbf{w}) \delta(\mathbf{r} - \mathbf{r}_0), \mathbf{r} \in \Gamma_1(\mathbf{r}), (\mathbf{n}_1, \mathbf{w}) < 0, \\ J(\mathbf{r}, \mathbf{w}) = 0, \mathbf{r} \in \Gamma_2(\mathbf{r}), (\mathbf{n}_2, \mathbf{w}) < 0, \end{cases} \quad (2)$$

where $S(\mathbf{r}, \mathbf{w})$ is the spatial-angular distribution of the irradiation. \mathbf{n}_1 and \mathbf{n}_2 are the inner normals to the surfaces $\Gamma_{1,2}(\mathbf{r})$ limiting the atmosphere from above and from below.

The solution of Eq. (1) under the boundary conditions (2) is the point spread function (PSF), or the pulse response of the channel of formation and transfer of the image. The relation between the fundamental solution of Eq. (1), i.e., – the Green’s function, and the point spread functions was considered in Ref. 10. One can write the solution of Eq. (1) for any specific distribution of the reflection (irradiation) ability set on the Earth’s surface under certain conditions (isoplanarity of the images, homogeneity of the Earth’s surface, etc.) by means of the PSF, using the superposition principle. Thus, the goal of the study is to determine the dependence of the pulse response on the variables of the problem.

In the case under consideration these are the composition of the atmosphere, spatial distribution of the optical properties of the medium, and irradiation of the atmosphere and the Earth’s surface.

To analyze the effect of an individual physical process on the natural radiation of the “atmosphere – underlying surface” recorded with the receiver, we have calculated the intensity J_λ and radiation temperature T_λ

$$\begin{aligned} J_\lambda &= J_\lambda^0 + J_\lambda^{\text{MS}}, \quad T_\lambda = B_\lambda^{-1} [J_\lambda], \\ J_\lambda^0 &= J_{\text{ATM}}^0 + J_{\text{SURF}}^0, \quad J_\lambda^{\text{MS}} = J_{\text{ATM}}^{\text{MS}} + J_{\text{SURF}}^{\text{MS}}, \\ J_{\text{SURF}}^0 &= B_\lambda [T_S(x_0, y_0)] \exp(-\tau), \\ J_{\text{SURF}}^{\text{MS}}(x_0, y_0) &= \iint_S h_\lambda(x - x_0; y - y_0) B_\lambda [T_S(x, y)] dx dy. \end{aligned}$$

Here J_{ATM}^0 , J_{SURF}^0 , J_λ^{MS} and $J_{\text{SURF}}^{\text{MS}}$ are the contributions of the atmosphere and the underlying surface into the intensities of direct (J_λ^0) and scattered (J_λ^{MS}) radiation; τ is the optical thickness of the atmosphere; B_λ is the Plank function; B_λ^{-1} is the inverse Plank function; T_S is the temperature of the underlying surface; $h(x - x_0; y - y_0)$ is the point spread function; $(x_0; y_0)$ are the observation point coordinates; S is the effective area of the

adjacency effect formation. The area S in our calculations was limited by the circle with the center at the point $(x_0; y_0)$ and radius R . The value R was 300 km.

The solution of Eq. (1) under the boundary conditions (2) was obtained by the Monte-Carlo method, that allowed to take into account all processes participating in the formation and transfer of the Earth's surface image through the atmosphere asymptotically accurately.

The algorithm of the local estimate on the conjugate trajectories¹¹ was used in the calculations

$$h(x, x_0; y, y_0) = \frac{1}{M} \sum_{k=1}^M \xi_k, \quad \xi_k = \sum_{n=0}^{N_k} \Psi(X_n).$$

The local estimate had the form

$$\Psi(X_n) = \Lambda_n g_{nj} \exp\{-\tau_{nj}\} \mu_{nj}/2\pi^2 r_{nj}^2.$$

Here M is the number of random trajectories, N_k is the number of collisions on the k -th trajectory, $X_n = (x_n, y_n, z_n, \mathbf{w}_n)$ are the coordinates and direction of the photon coming to the n -th collision

on an ordinary random trajectory, $\Lambda_n = \prod_{i=1}^n \omega_0(X_i)$,

$\omega_0(X_i)$ is the single scattering albedo at the point X_i , $g_{nj} = g\{\gamma(X_n, X_j)\}$ is the scattering phase function at the point X_n , $X_j = (x_j, y_j)$ is the point on the Earth's surface, $\gamma(X_n, X_j)$ is the cosine of the angle between \mathbf{w}_n and the direction toward the point X_j , $\tau_{nj} = \tau(X_n, X_j)$ is the optical distance from the point X_j to the point X_n , $\mu_{nj} = \mu(X_n, X_j)$ is the cosine of the angle between the normal to the surface at the point X_j and the direction to the point X_n , and $r_{nj} = r(X_n, X_j)$ is the distance from X_j to X_n .

The "integral" PSF $h_\lambda^*(\varphi) = \int_0^R h_\lambda(r, \varphi) r dr$ was

calculated for a convenience of the analysis of the spatial symmetry of the pulse reseonses. Here $h_\lambda(r, \varphi)$ is the function $h(x - x_0, y - y_0)$ in the polar coordinates (r, φ) , where r is the distance from (x_0, y_0) to an arbitrary point (x, y) on the Earth's surface; φ is the azimuth angle, and $\tan \varphi = (x - x_0)/(y - y_0)$.

Investigations were carried out for the following models of the optical properties of the atmosphere and the Earth's surface and the optical and geometrical parameters of the observation pattern:

- spectral channels at $\lambda = 3.75$ and $10.8 \mu\text{m}$;
- zenith angles of the path (from the horizon) $\Theta = 30\text{--}90^\circ$;
- cloudless atmosphere, molecular-plus-aerosol, spherically symmetric, vertically stratified, and horizontally uniform;
- upper boundary at the altitude of 100 km;

- meteorological model of the midlatitude summer and winter;

- aerosol models (two situations):

- 1) continental (rural) or urban aerosol in the near-ground atmospheric layer up to 2 km (meteorological range $S_M = 1\text{--}50$ km) and the background aerosol content in the troposphere and the stratosphere;

- 2) the transparent atmosphere in the near-ground layer and different models of the stratospheric aerosol layers, which have maximum extinction at the altitudes of 14–20 km;

- model of the underlying surface of a Lambertian type, irradiated according to the black body law at a temperature $T_S = 294.2$ K and 272.2 K for the summer and winter, respectively.

Vertical profiles of the meteorological parameters of the atmosphere, molecular and aerosol extinction (scattering) coefficients were obtained based on the data from the LOWTRAN-7 software complex.¹²

3. RESULTS OF MODELING

3.1. Contribution of Scattering into the Formation of the Upwelling Thermal Flux

The effect of light scattering properties of atmospheric aerosol on the intensity of upwelling IR radiation in the case of homogeneous underlying surface is illustrated in Figs. 2–4, the analysis of which allows to draw the following conclusions.

The scattering by aerosol can play a noticeable role in the formation of the upwelling fluxes of thermal radiation under the conditions of a turbid atmosphere. Its relative contribution $R_{\text{SCT}} = J_\lambda^{\text{MS}}/J_\lambda$ into the intensity of outgoing thermal radiation monotonically increases as τ_{aer} increases (Fig. 2) and can reach 15–40% ($\lambda = 3.75 \mu\text{m}$) and 10–25% ($\lambda = 10.8 \mu\text{m}$) in the case of the near-ground aerosol. The value R_{SCT} noticeably decreases and does not exceed 6–18% in the case of volcanic aerosol. It is worth noting that there exist noticeable season differences in the values of relative contribution of scattered radiation for the near-ground aerosol. Moreover good coincidence of the "winter" curves $R_{\text{SCT}}(\tau_{\text{aer}})$ for $\Theta = 45$ and 90° is very attractive. Thus, one can suppose that the value R_{SCT} in these situations is determined only by the value of the aerosol optical thickness along the observation path. By comparing the calculational data for rural and urban aerosol (Fig. 2), one should note their noticeable difference (up to 5–15%), which is explained by the essential difference in the single scattering albedo of these aerosols. The spread of R_{SCT} for different meteorological models of the atmosphere is less than 0.5% in the case of volcanic aerosol at fixed values τ_{aer} , i.e. the value of the relative contribution of scattered radiation is determined only by the value of the aerosol optical thickness (Fig. 2).

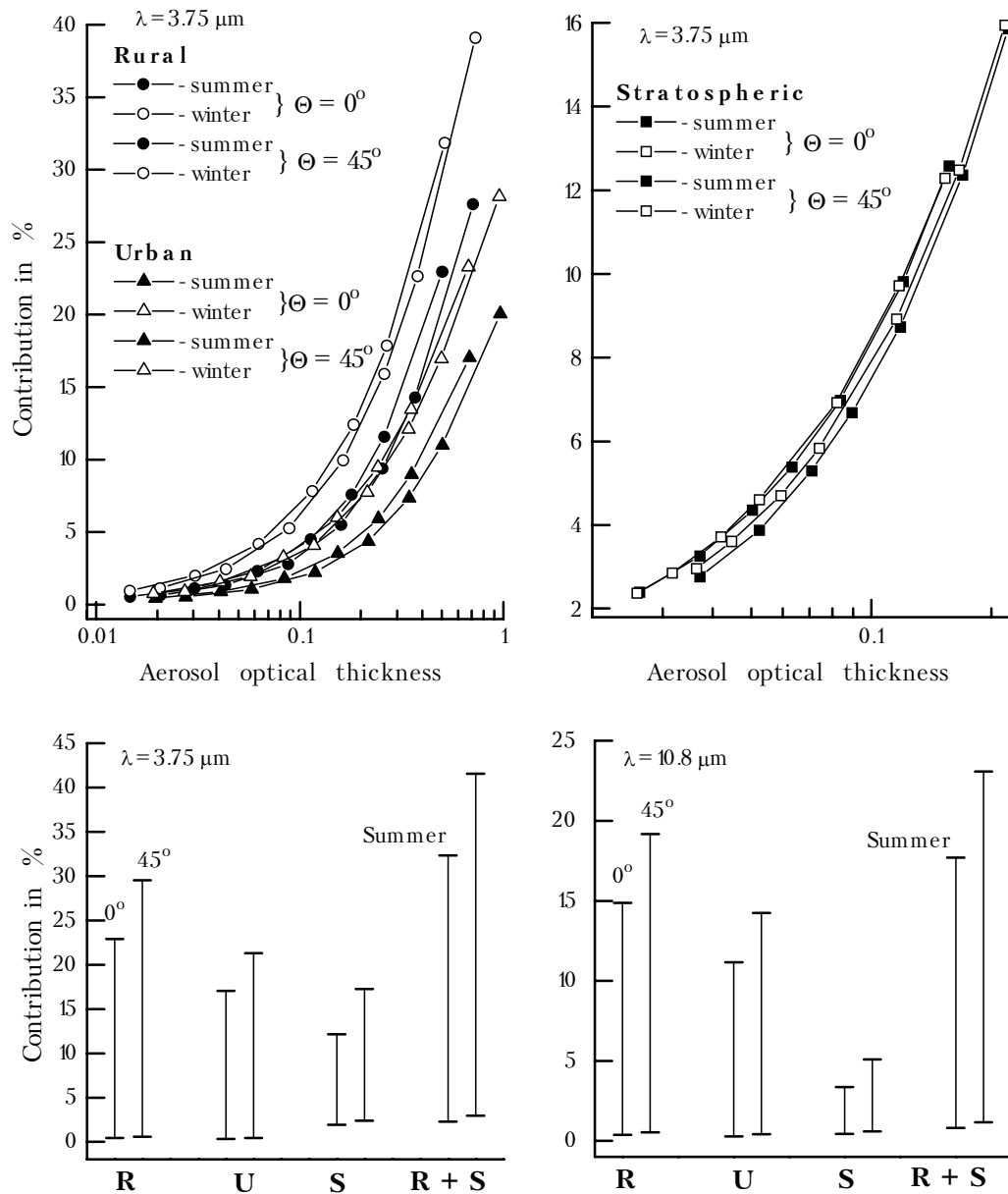


FIG. 2. Dependence of R_{SCT} on aerosol optical thickness and the ranges of its variability for different aerosol models (R – rural, U – urban, S – stratospheric).

The analysis of the data shown in Fig. 3 allows one to state the dominating role of the underlying surface in the formation of scattered radiation independently of the observation conditions. The value $R_{SRF} = J_{SURF}^{MS} / J_{\lambda}^{MS}$ increases at the enhanced aerosol concentration in the near-ground layer and the transparent stratosphere as the transparency of the atmosphere increases being in the ranges 50–85% (midlatitude summer) and 60–95% (midlatitude winter). In the presence of volcanic aerosol in the stratosphere this value exceeds 50% and 75–90% ($\lambda = 3.75 \mu\text{m}$) and 50–80% ($\lambda = 10.8 \mu\text{m}$). However, different from the case of near-ground aerosol, here it is weakly depends on τ_{aer} .

The results of estimation of a contribution from the multiply scattered radiation into J_{λ}^{MS} , when the number of the photon collisions with aerosol particles $n > 1$, can be of practical interest. Let us write the intensity of scattered radiation in the form $J_{\lambda}^{MS} = J_{\lambda}^{MS}(n = 1) + J_{\lambda}^{MS}(n > 1)$. The value $R_{MLT} = J_{\lambda}^{MS}(n > 1) / J_{\lambda}^{MS}$ is shown in Fig. 4. By comparing Fig. 2 and Fig. 4, one can see qualitative coincidence of the dependences of R_{MLT} and R_{SCT} on the optical and geometrical parameters of the image formation and transfer channel. It follows from the data shown in Fig. 4 that the contribution from single scattering into J_{λ}^{MS} dominates. However, the value R_{MLT} at the

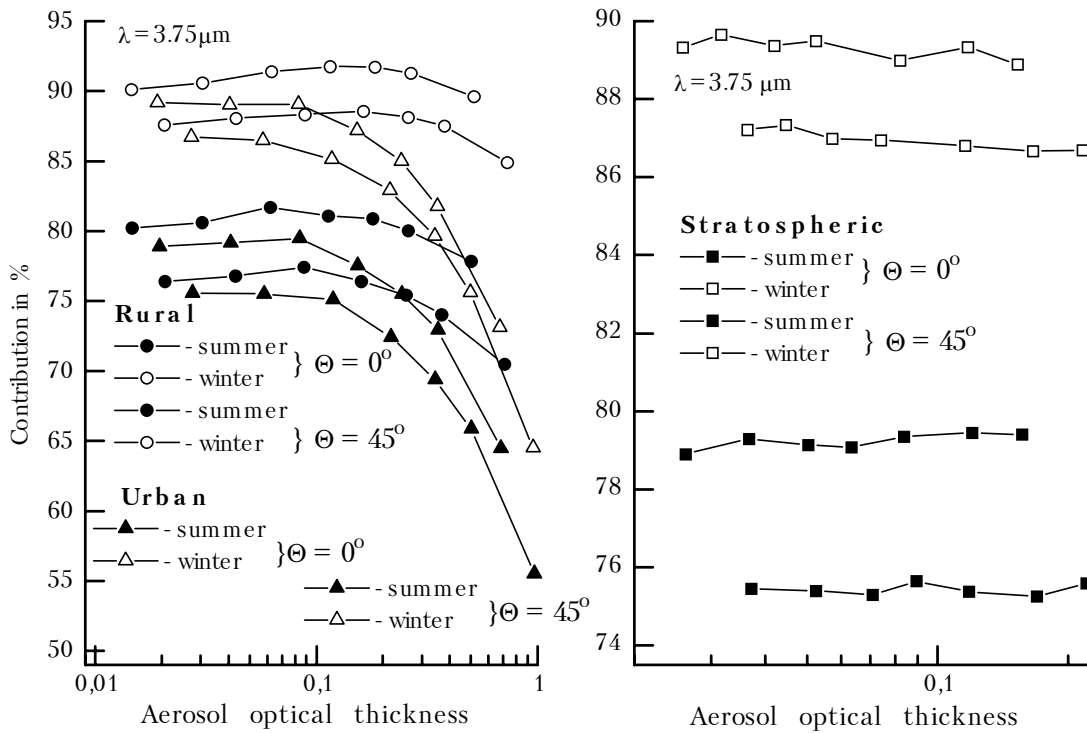


FIG. 3. Dependence of R_{SCT} on aerosol thickness for different aerosol models.

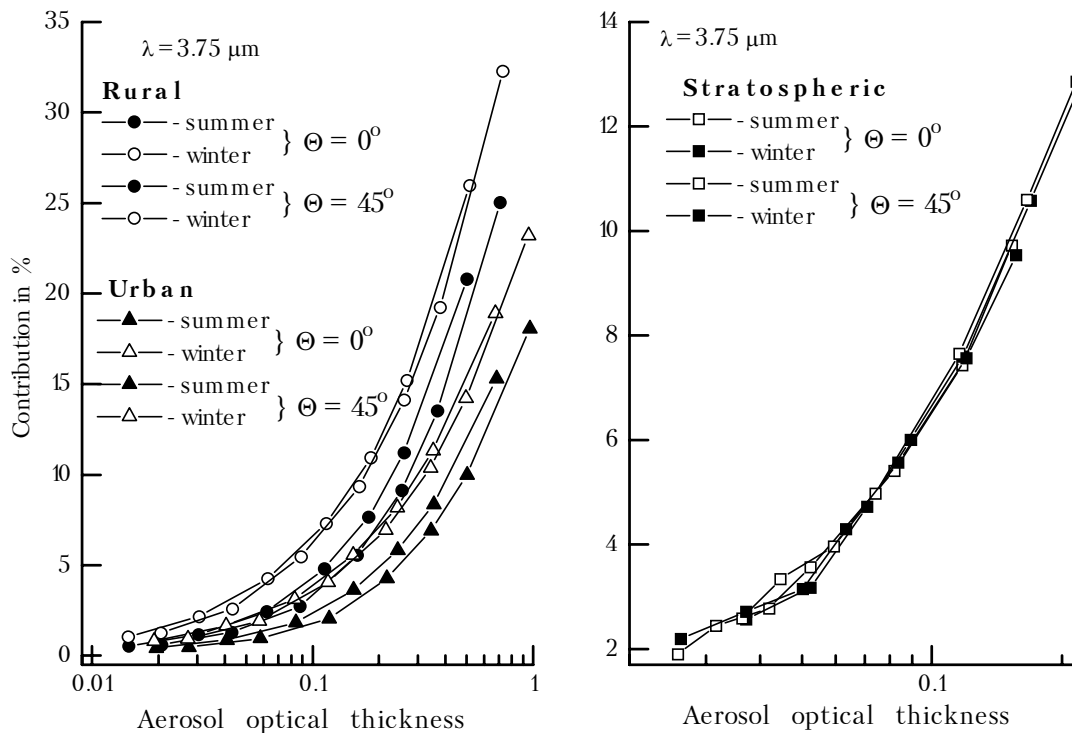


FIG. 4. Dependence of R_{MLT} on aerosol optical thickness for different aerosol models.

enhanced aerosol concentration in the near-ground atmospheric layer can reach 15–35% at $\lambda = 3.75 \mu\text{m}$ and 10–20% at $\lambda = 10.8 \mu\text{m}$. These values for these spectral channels are equivalent to the change

of radiation temperature δT by 0.6–3.0 K and 0.7–2.5 K. This value does not exceed 5–15% and corresponds to $\delta T < 0.5\text{--}0.6 \text{ K}$ for an enhanced volcanic aerosol concentration in the stratosphere

and clear troposphere. Let us consider the contribution of radiation multiply scattered in the atmosphere into J_{λ}^{MS} . It reaches a noticeable level ($\delta T_{\lambda} > 0.5$ K) for near-ground aerosol only at small zenith angles and meteorological visual range $S_M < 2$ km. This fact allows one to take into account single scattering when modeling the atmospheric radiation scattered by the aerosol for solving some practical problems.

3.2. Modeling of the Pulse Response

Let us analyze the spatial properties of the point spread function.

3.2.1. Near-ground aerosol

The general view of the spatial distribution of the PSF is shown in Fig. 5. The function $h(r)$ in the

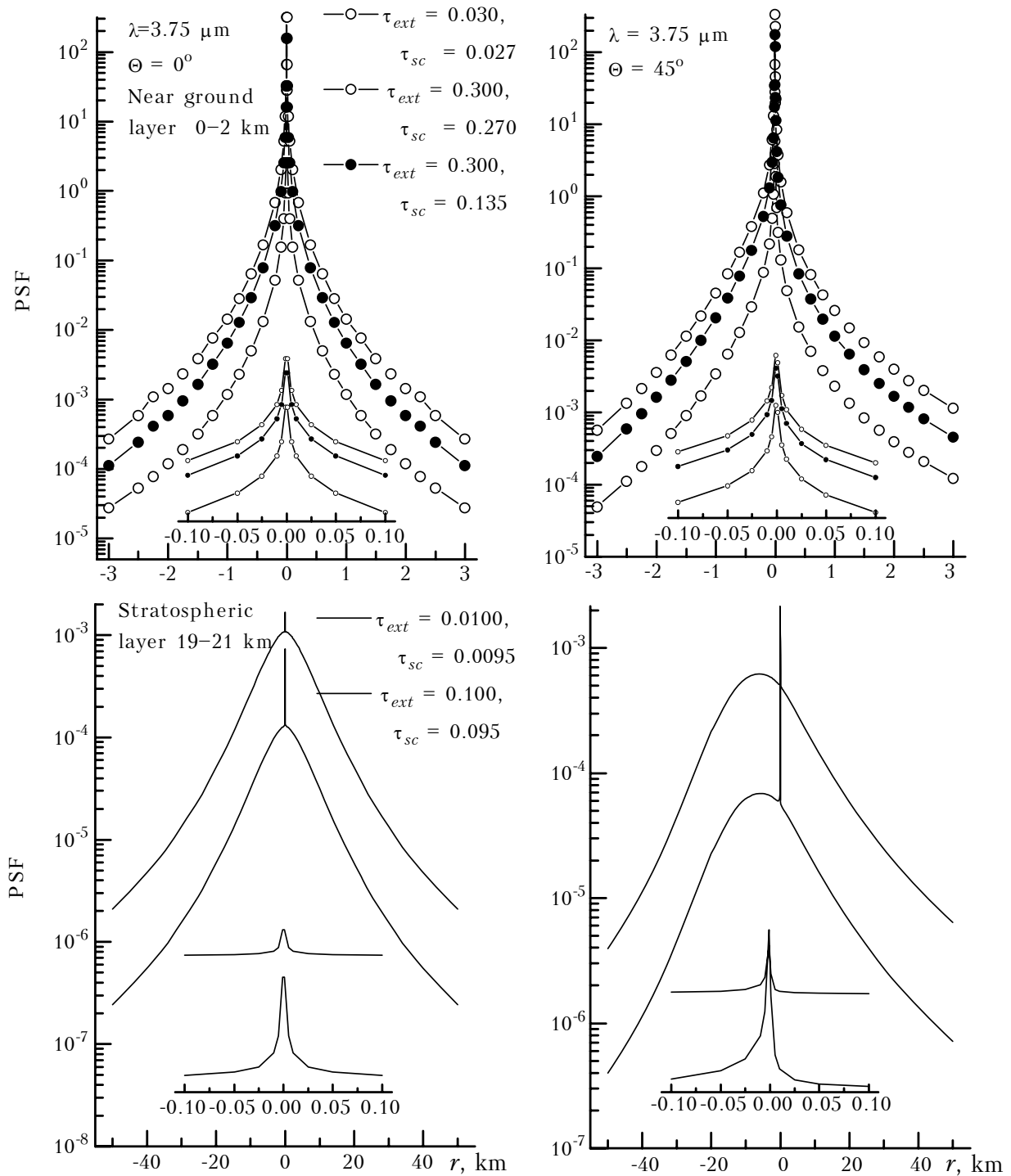


FIG. 5. Spatial distribution of the PSF in YOZ plane for different aerosol models.

considered distance range $r < 20$ km monotonically and quickly decreases as r increases. Figure 5 also illustrates quite an evident fact that the point spread function in the case of nadir observation ($\Theta = 90^\circ$) has circular symmetry. The axial symmetry of the PSF is broken when observing along a slant path: while it keeps the symmetry relative to the YOZ plane, the plot of the function $h_\lambda(x, y)$ elongates

along to the OY axis toward negative values (to the observer). The degree of asymmetry of $h_\lambda(x, y)$ is visually illustrated by the data on the integral PSF $h^*(\varphi)$ in the case of $\Theta = 45^\circ$ shown in Fig. 6. The analysis of this function allows one to isolate the following peculiarities in its behavior: a) the presence of the minimum at the azimuth value $\varphi \approx 60-75^\circ$; b) its significant (several times) increase with the value φ

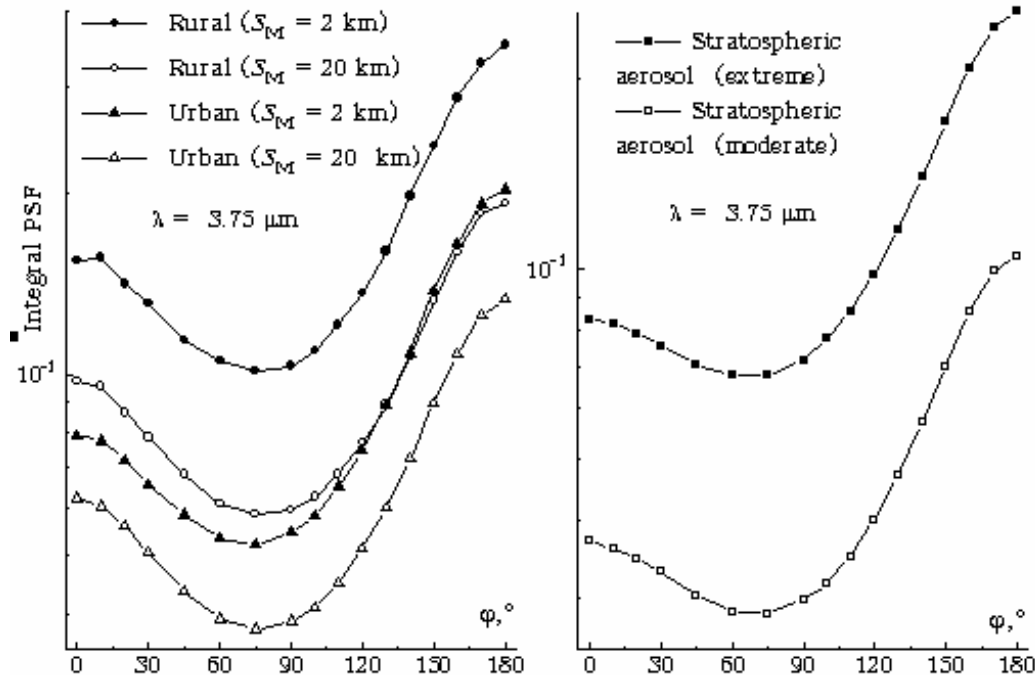


FIG. 6. Dependence of the integral PSF on azimuth angle for different aerosol models.

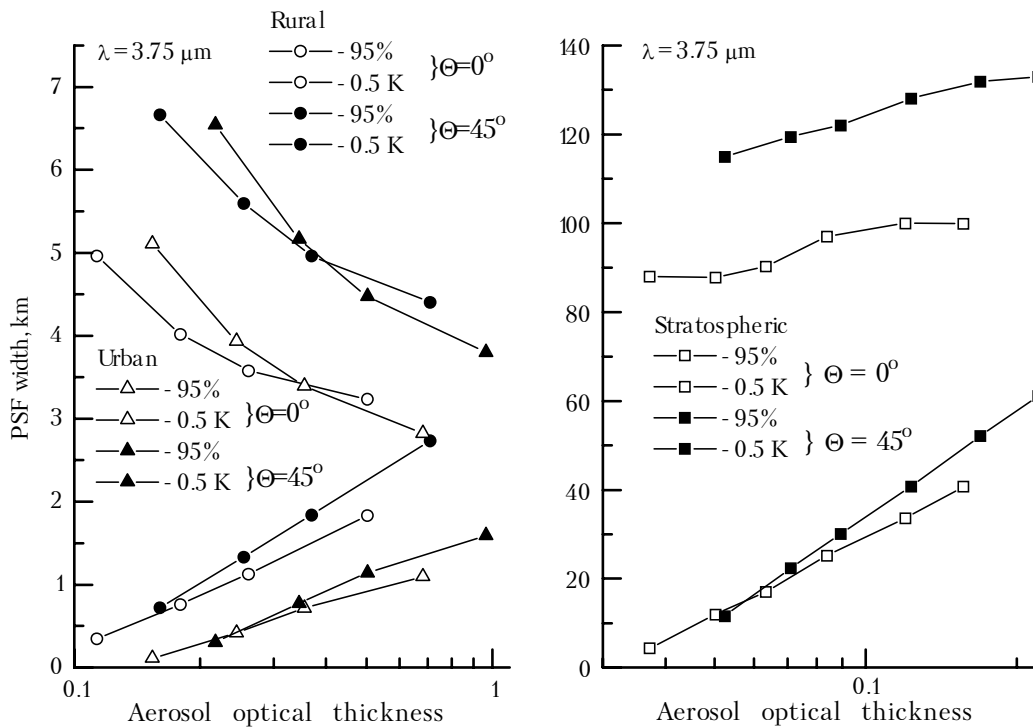


FIG. 7

increase. Thus, the character of the PSF asymmetry has other peculiarities in addition to the general elongation, and its degree can reach significant value.

Analysis of the dependence of the point spread function on the optical thickness reveals the monotonic increase of the PSF values as τ_{aer} increases. Then the good coincidence of the angular dependence $h^*(\varphi)$ is observed at different values of the single scattering albedo and the aerosol optical thickness, and the following relationship holds:

$$\frac{h(x - x_0, y - y_0; \tau_1)}{h(x - x_0, y - y_0; \tau_2)} \approx \text{const}.$$

This property of the PSF means that its spatial shape keeps unchanged when changing τ_{aer} and the optical characteristics of aerosol scattering within the limits considered.

The width of the point spread function at the integral level of 95% and the error in calculating radiative temperature $\delta T_\lambda = 0.5$ K is illustrated by the data in Fig. 7.

3.2.2. Postvolcanic aerosol

To study the peculiarities of the pulse response of IR channels at the presence of a scattering layer in the stratosphere, the aerosol model of the layer located in the stratosphere was considered. The results of modeling of the PSF spatial distribution for stratospheric aerosol are shown in Fig. 5. The analysis of these data allows one to speak about, similar, on the whole, (with the case of near-ground aerosol) dependence of the point spread function on τ_{aer} , and in particular, about constant shape of $h(x, y)$ at changing optical thickness.

As to the near-ground aerosol, the break of the axial symmetry of the PSF when observing along slant paths takes place here. However, in this case the asymmetry has a peculiarity. The break of monotonic character of the dependence $h(r)$ is observed at $y < 0$, and formation of a well pronounced maximum occurs in the YOZ plane, and its distance from the point of observation depends on the observation angle and the altitude, where the scattering layer occurs

$$r_{\text{max}} \sim z_{\text{aer}} \cot \Theta,$$

where z_{aer} is the altitude of the scattering layer center above the Earth's surface. It is easy to obtain this estimate of the maximum position from the expression for the intensity of the adjacency effect in the single scattering approximation at slant observation of a uniform Lambertian surface through the scattering layer.

Let us pay attention to the invariant behavior of the PSF shape with respect to the variations of τ_{aer} . It is quite sufficient to determine the "scaling" factor

for each value Θ , $k \sim \tau_{\text{aer}}/\tau_0$ which makes it possible to calculate the point spread function $h(\tau_{\text{aer}}, x, y)$ for the τ_{aer} value required from the data on $h(\tau_0, x, y)$ without any additional modeling of its spatial shape. Thus, one can noticeably reduce the amount of calculations at multiple modeling of the pulse response of the channels of IR radiation propagation under conditions of spatiotemporal variability of the aerosol optical properties.

4. APPLICATIONS

Satellite observations of the temperature-inhomogeneous Earth's surface by means of IR channels of the AVHRR radiometer were simulated in the numerical experiments for spectral channels: at $\lambda = 3.75$ and $10.8 \mu\text{m}$ and the observation point altitude: $H_0 = 800$ km and the area of the element of the spatial resolution of the device: $S_0 \approx 1.0 \text{ km}^2$ at $\Theta = 0^\circ$ and $S_0 \approx 4.0 \text{ km}^2$ at $\Theta = 45^\circ$.

4.1. Large-Scale Gradients

The model of a nonuniform underlying surface was set as follows. Let the line pass through the area of the adjacency effect formation, and divides this area into two uniform Lambertian parts emitting according to the black body law at temperatures T_S (area S_1) and $T' = T_S + dT_S$ (area S_2), the observation point (x_0, y_0) is in the area S_1 . Temperature of the observation point is $T_S = 294.2$ K. The temperature gradient dT_S varies in the range from -20 to 20 K. The model is characterized by two geometrical parameters, the distance d between the dividing line and the point (x_0, y_0) ; and the azimuth angle β between the projection of the optical axis of the receiver on the underlying surface and the dividing line, or the angle $\varphi = 90^\circ - \beta$ that corresponds to the azimuth angle φ in the point spread function.

The results of investigations are presented in the form of the temperature corrections

$$\delta T_\lambda = T_\lambda|_{dT_S = 0} - T_\lambda|_{dT_S \neq 0}$$

depending on the parameters of temperature inhomogeneities r and T_S for different optical and geometrical conditions of the observation.

The value of temperature corrections in the channel $\lambda = 10.8 \mu\text{m}$ does not exceed 0.5° for the maximum τ_{aer} values and dT_S . One can neglect the distorting adjacency effect when performing the atmospheric correction of remote measurement data in this channel, therefore below we present only the results of modeling for the channel at $\lambda = 3.75 \mu\text{m}$.

The temperature corrections $\delta T_\lambda(d)$ calculated for different angles Θ and φ is shown in Fig. 8. When analyzing these data, it is necessary to pay special attention to the following circumstance. The noticeable asymmetry of the point spread function in

the case of slant paths of observation leads to the azimuth dependence of the temperature corrections (on the angle φ). Their values at $\varphi = 0$ and 180° can differ by more than 1° (Fig. 9). The width of the

zone where this difference is more than 0.5° for the maximum values τ_{aer} and $dT_S = 20^\circ$, reaches 0.5 km for the near-ground aerosol and 15 km for the postvolcanic aerosol.

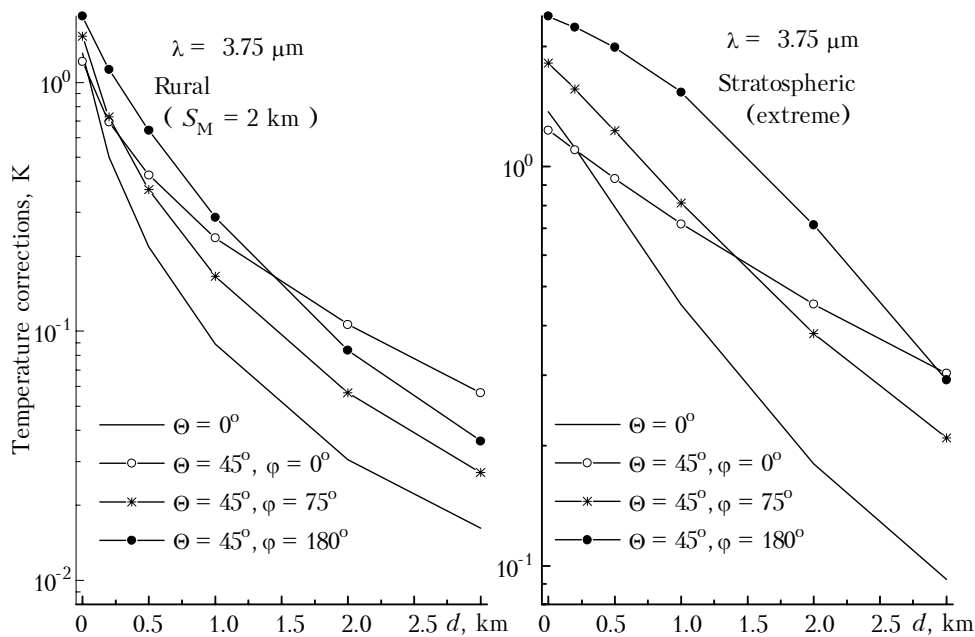


FIG. 8. The temperature correction as a function of distance for different angles Θ and φ .

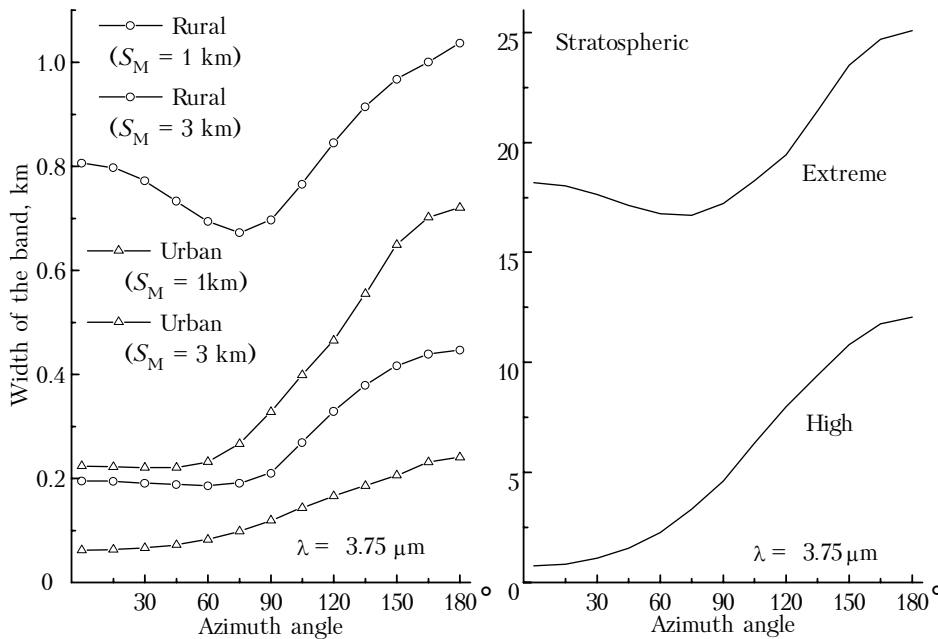


FIG. 9. Dependence of width of the band (d_{max}) on azimuth angle for different aerosol models.

In parallel with this fact, the results of estimation of the value d_{max} , which satisfies the condition $\delta T_\lambda(d) < 0.5^\circ$ at $d > d_{max}$ can be of practical interest. These data are shown in Fig. 9.

The process of aerosol scattering leads to the “spread” of the gradient line of the temperature inhomogeneous images.

The band appears on both sides of the dividing line, in the limits of which the results of remote measurements can noticeably differ, depending on the observation point and orientation of the optical axis of the device. The width of this band is determined by the degree of atmospheric turbidity, the temperature gradient value, and can reach the value of the order of 1–20 km (depending on the

altitude of the scattering layer). This conclusion should be taken into account when performing the atmospheric correction of the remote temperature measurement results of high and moderate spatial resolution, obtained, for example, in the coastal zone.

4.2. High-Temperature Anomalies

The model of the underlying surface was set as follows. Let the element of the area S_0 be on the

underlying surface. The high-temperature part of the surface of the area $S_H < S_0$ and temperature T_H is assumed to be at its center.

The value $S_H = L_H \times L_H$ is the linear size of the high-temperature inhomogeneity. For instance, a fire may vary in from 10×10 to 1000×1000 m².

Let the fire temperature is $T_H = 600$ and 1000 K, that corresponds to the smoldering and burning processes, respectively. Temperature of the surrounding surface is $T_S = 294.2$ K.

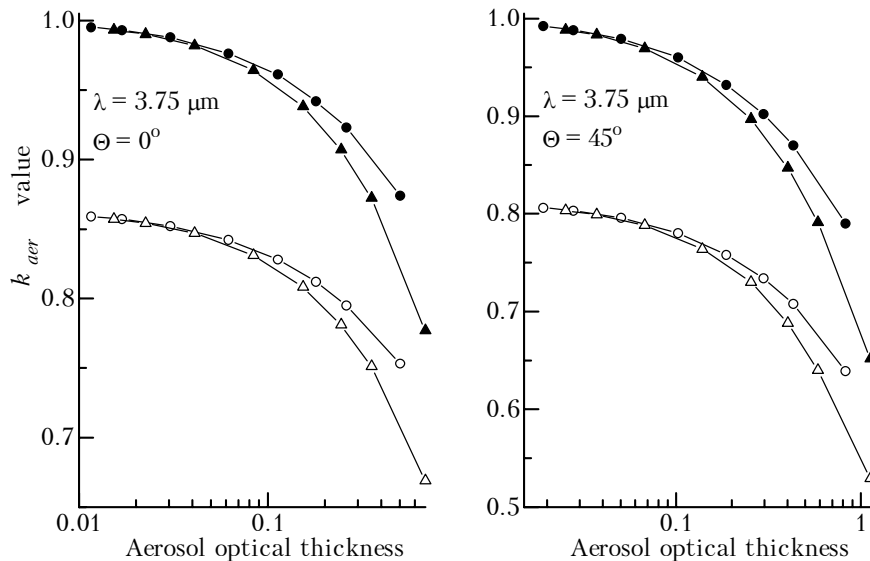


FIG. 10. Dependence of k_{aer} value on aerosol optical thickness for different models: rural aerosol (—●—), rural aerosol and molecular extinction (—○—), urban aerosol (—▲—), urban aerosol and molecular extinction (—△—).

The intensity of the thermal radiation (brightness temperature) was averaged over the area S_0

$$\bar{J}_\lambda = J_{ATM} + \frac{1}{S_0} \iint_{S_0} J_{SURF}(x, y) dx dy,$$

$$\bar{T}_\lambda = B_\lambda^{-1} [\bar{J}_\lambda].$$

Let us now formulate the major results of the investigations (Fig. 10).

a) The analysis of k_{aer} values (the error in estimating the linear size) shows that noticeable errors leading to underestimating the value L_H by 20–60% from the satellite data (the area S_H by 1.5–2.5 times), may appear if under conditions of high turbidity of the atmosphere the distorting effect of aerosol in the near-ground layer is neglected.

b) The stratospheric aerosol layer affects the measured value, in the presence of the small-scale high-temperature anomalies much weaker (in comparison with the near-ground one). Then, even in the case of the extremum (of the considered variants) aerosol content in the stratosphere the error in remote estimation of the fire linear size does not exceed 15%, and 30% in its area.

c) The degree of distortion of the high-temperature fire size is mainly determined by the aerosol optical thickness, i.e. the portion of scattered radiation $R_{SCT} = J_\lambda^{MS} / J_\lambda$ may be neglected.

Thus, the distorting effect of aerosol under the conditions of high turbidity of the near-ground atmospheric layer may seriously hinder seeking of a reliable solution to the problem of detecting small-scale high-temperature anomalies (fires) and determining their temperature and size from the aerospace IR data of a moderate spatial resolution.

REFERENCES

1. K.Ya. Kondrat'jev, O.I. Smoktii, and V.V. Kozoderov, *Effect of the Atmosphere on the Study of Natural Resources from Space* (Mashinostroenie, Moscow, 1985), 272 pp.
2. V.V. Belov, *Atm. Opt.* **2**, No. 8, 649–660 (1989).
3. B.S. Zhukov, *Kosmicheskii Bulletin* **2**, No. 2, 5–8 (1995).
4. S.V. Afonin, V.V. Belov, and I.Yu. Makushkina, *Atmos. Oceanic Optics* **7**, No. 6, 423–429 (1994).
5. S.V. Afonin, V.V. Belov, and I.Yu. Makushkina, *ibid.*, 430–434.
6. S.V. Afonin, V.V. Belov, and I.Yu. Makushkina, *ibid.*, 435–440.

7. S.V. Afonin, V.V. Belov, and I.Yu. Makushkina, *Atmos. Oceanic Optics* **8**, No. 9, 756–762 (1995).
8. S.V. Afonin, V.V. Belov, and I.Yu. Makushkina, *Atmos. Oceanic Optics* **8**, No. 12, 1013–1019 (1995).
9. S.V. Afonin, V.V. Belov, and I.Yu. Makushkina, *Atmos. Oceanic Optics* **10**, No. 2, 114–118 (1997).
10. V.V. Belov, *Atmos. Oceanic Optics* **5**, No. 8, 535–538 (1992).
11. V.V. Belov and I.Yu. Makushkina, in: *Theory and Applications of Statistical Modeling* (Computing Center of Siberian Branch of the Russian Academy of Sciences, Novosibirsk, 1988), pp. 153–164.
12. F.X. Kneizys, E.P. Shettle, L.W. Abreu, et al., *User's Guide to LOWTRAN-7*. AFGL-TR-88-0177. ERP. No. 1010. AFGL, Hanson AFB, MA 01731 (1988).